Provided for non-commercial research and education use.
Not for reproduction, distribution or commercial use.

This article appeared in a journal published by Elsevier. The attached copy is furnished to the author for internal non-commercial research and education use, including for instruction at the authors institution and sharing with colleagues.

Other uses, including reproduction and distribution, or selling or licensing copies, or posting to personal, institutional or third party websites are prohibited.

In most cases authors are permitted to post their version of the article (e.g. in Word or Tex form) to their personal website or institutional repository. Authors requiring further information regarding Elsevier's archiving and manuscript policies are encouraged to visit:

http://www.elsevier.com/authorsrights

Author's personal copy

Journal of Alloys and Compounds 604 (2014) 352–362

Contents lists available at ScienceDirect

Journal of Alloys and Compounds

journal homepage: www.elsevier.com/locate/jalcom

Effect of alkali-earth modifier ion on electrical, dielectric and spectroscopic properties of Fe_2O_3 doped Na_2SO_4—MO—P_2O_5 glass system

L. Pavić [a], A. Moguš-Milanković [a], P. Raghava Rao [b,c], A. Šantić [a], V. Ravi Kumar [b], N. Veeraiah [c,*]

[a] Ruđer Bošković Institute, Zagreb, Croatia
[b] Department of Physics, Krishna University-Dr. M.R.A.R. Campus, Nuzvid 521 201, AP, India
[c] Department of Physics, Acharya Nagarjuna University, Nagarjuna Nagar 522 510, AP, India

ARTICLE INFO

Article history:
Received 14 February 2014
Received in revised form 7 March 2014
Accepted 10 March 2014
Available online 20 March 2014

Keywords:
Phosphate glasses
Dielectric dispersion
Electrical conductivity
Spectroscopic properties

ABSTRACT

Sodium sulfo-phosphate glasses mixed with three different modifier oxides (MgO, CaO and BaO) and doped with 1.0 mol% of Fe_2O_3 were synthesized. The combined analysis of optical absorption and ESR spectroscopy has indicated that the iron ions exist in both Fe^{3+} (in octahedral and/or tetrahedral) and Fe^{2+} (in octahedral) local coordination sites. The results of Raman spectral studies have shown a higher degree of disorder for BaO containing glass and electrical studies have revealed the highest electrical conductivity for this glass. This is related to the higher depolymerization of the glass network by Ba^{2+} ions owing to its larger ionic radius which in turns causes a decrease in electrostatic binding energy and strain energy for an easy passage of sodium ions. The low conductivity observed for all glasses is a result of the interaction between sodium and alkaline-earth ions which can be classified as the "mixed alkali–alkaline earth" effect.

© 2014 Elsevier B.V. All rights reserved.

1. Introduction

The study of dielectric properties such as dielectric permittivity $\varepsilon'(\omega)$, loss $\tan\delta$ and ac conductivity, σ_{ac}, over a wide range of frequencies and temperatures not only helps in accessing the insulating character and understanding the conduction phenomenon of the glass materials but also throws information on their structural aspects. In this context, a large number of studies on a variety of inorganic glass materials have been reported recently giving valuable structural information [1–6]. In particular, relationship among composition, structure and electrical properties of alkali/alkaline sulfo-phosphate glasses are of special interest due to their applicability as electrolytes especially in high temperature solid-state sodium–sulfur batteries [7]. Also, these glasses have been widely used to integrate radioactive waste for long time safe storage [8]. Therefore, it is of the interest to investigate the behavior of sulfur in the phosphate glass system.

Various phosphate glasses may have the capacity to dissolve moderate level of sulfur species [8], which can interact weakly with metaphosphate units. Such a weak interaction results in a small dynamic concentration of dithiophosphate (DTP) units [9]. Data on iron phosphates suggest moderate sulfate solubility but most of these glasses contained substantial level of alkali oxides [8,10].

It is well known that the incorporation of alkaline-earth oxides, such as MgO, CaO and BaO, into the glass matrix leads to a disruption of the glass network and promotes the formation of non-bridging oxygens (NBO) groups [11]. The ionic field strengths I ($I = z/r^2$ where z is the charge number and r is the ionic radius) for Mg^{2+}, Ca^{2+} and Ba^{2+} ions are 4.73 $Å^{-2}$, 2.04 $Å^{-2}$ and 1.49 $Å^{-2}$, respectively, resulting in a more strongly bonded structure due to the greatest field strength of the Mg^{2+} and Ca^{2+} as compared to Ba^{2+} [12]. Therefore, when sodium sulfate-phosphate glasses are mixed with these network modifying ions the structural modifications are expected to occur influencing the electrical properties.

Among various transition metal ions, iron ions have a strong bearing on electrical and optical properties of glasses. A large number of interesting studies are available on the environment of iron ions in various inorganic glass systems, such as phosphate, silicate, borate, arsenate and germanate glasses [13–18]. In general, the content of iron ions in different environments and in different valence states in the glass depends on the quantitative properties of modifiers and glass formers, size of the other ions in the glass structure, their field strength, mobility of the modifier cation, etc.

* Corresponding author. Tel.: +91 863 2346174; fax: +91 863 2293378.
E-mail address: nvr8@rediffmail.com (N. Veeraiah).

http://dx.doi.org/10.1016/j.jallcom.2014.03.061
0925-8388/© 2014 Elsevier B.V. All rights reserved.

Author's personal copy

In phosphate glasses iron ions exist as Fe^{3+} in both tetrahedral and octahedral coordination and as Fe^{2+} in octahedral environment [19]. Due to the existence of iron ions in different valence states, these glasses are identified as electron conductors with polaronic conduction mechanism. Electronic conduction takes place by electron hopping from Fe^{2+} to Fe^{3+} ions and strongly depends on Fe_2O_3 content, redox ratio, Fe^{2+}/Fe_{tot}, and average distance between iron ions [20,21]. On the other hand, phosphate glasses containing both iron and mobile alkali ions exhibit mixed ionic-polaronic conductivity [22].

In earlier studies, we have reported the influence of MgO, CaO and BaO modifier oxides on emission characteristics and luminescence efficiencies of different rare earth ions (Sm^{3+}, Ho^{3+} and Er^{3+} ions) in Na_2SO_4—P_2O_5 glasses [23,24]. More recently [25], we have investigated the influence of Fe_2O_3 addition on the electrical properties of the Na_2SO_4—BaO—P_2O_5 glasses. The obtained results indicated that there is a mixed conduction, ionic and electronic, present in these glasses. It was also found that their contributions to the total electrical conductivity are affected by the amount of the added Fe_2O_3.

The present investigation is aimed to provide a comprehensive understanding over the influence of three network modifiers, MO=MgO, CaO and BaO, on the electrical properties of the Na_2SO_4—MO—P_2O_5 glasses doped with 1.0 mol% of Fe_2O_3 and to identify the best modifier oxide that makes the glass to exhibit more electrical conductivity. In addition these studies assist in understanding the conduction phenomenon and also give deeper information on the structural changes taking place in the glass network due to the variation of the modifier oxide. Thus the purpose of this study is to throw some light on the relationship between the structural modifications in the glass network and electrical properties with the aid of the data from spectroscopic studies: optical absorption, ESR and Raman spectroscopy.

2. Experimental

Within the glass forming region of the Na_2SO_4—MO—P_2O_5 system, the following batch composition, in mol%, were chosen for the present study:

BF_{10} : $19.0Na_2SO_4$—$20.0BaO$—$60.0P_2O_5$: $1.0Fe_2O_3$

CF_{10} : $19.0Na_2SO_4$—$20.0CaO$—$60.0P_2O_5$: $1.0Fe_2O_3$

MF_{10} : $19.0Na_2SO_4$—$20.0MgO$—$60.0P_2O_5$: $1.0Fe_2O_3$

Analytical-grade reagents of Na_2SO_4, $MgCO_3$, $CaCO_3$, $BaCO_3$, $(NH_4)H_2PO_4$ and Fe_2O_3 powders in appropriate amounts were thoroughly mixed in an agate mortar and melted using a thick-walled platinum crucible at about 1173 K in a PID temperature-controlled furnace for about 1 h. The resultant bubble-free melt was then poured in a brass mould and subsequently annealed at 573 K. The amorphous nature of the samples was monitored by X-ray diffraction and scanning electron microscopy techniques. Afterwards, the samples were optically polished to the average dimensions of 1.0 cm × 1.0 cm × 0.2 cm.

As per the procedure described in our earlier paper [25], The EDS analysis of the glass samples indicated that the final concentrations of the elements viz., O, M, S, Na, Fe and P elements in the final glass are well intact in all the glass samples. The error estimated to be less than ±3%.

Differential scanning calorimetric (DSC) studies on the samples was carried out using Mettler Toledo DSC1 STARe system. Heating rate was maintained at 10 K/min within temperature range 300–1100 K. The density of the glasses was determined to an accuracy of (±0.0001) by the standard principle of Archimedes' using o-xylene (99.99% pure) as the buoyant liquid. The mass of the samples was measured to an accuracy of 0.1 mg using Ohaus digital balance Model AR2140 for evaluating the density.

The Electron Spin Resonance (ESR) spectra of the fine powders of the samples were recorded at room temperature on JEOL X-band (ν = 9.5 GHz) ESR spectrometer. The Raman spectra of the samples were recorded with an 10 ns Nd:YAG laser line (1064 nm) with a resolution of 1.0 cm^{-1} using Nicolet 6700 Raman spectrometer equipped with an FT Raman supplementary accessory working in a back-scattering geometry system. The optical absorption spectra of the glasses were recorded to a resolution of 0.1 nm at room temperature in the spectral wavelength range covering 300–1050 nm using JASCO Model V-670 UV–vis-NIR spectrophotometer.

For the electrical/dielectric measurements the gold electrodes were sputtered onto both sides of the samples using Sputter Coater SC7620. Dielectric properties were obtained by measuring complex impedance using an impedance analyzer (Novocontrol Alpha-AN Dielectric Spectrometer) over a frequency range from 0.01 Hz to 1 MHz and in temperature range from 303 to 523 K. The temperature was controlled to an accuracy of ±0.5 K. The impedance spectra were analyzed by means of equivalent circuits modeling and parameters were obtained using a complex non-linear least square (CNLLSQ) fitting procedure.

3. Results

3.1. Thermal, optical and structural analysis

It was ensured that the glasses prepared were free from visible inhomogeneities such as inclusions, cracks or bubbles. Based upon the XRD analysis it was confirmed that there is no crystalline phases present in the glass samples prepared.

From the measured values of the density, D, and average molecular weight, $\overline{M}$, of the samples, various other physical parameters such as iron ion concentration N_i, mean iron ion separation, R_i, polaron radius, R_p, are calculated and presented in Table 1.

In Fig. 1 the DSC scans for the Na_2SO_4—P_2O_5 glasses containing BaO, CaO and MgO doped with 1.0 mol% of Fe_2O_3 are presented. The small endothermic peaks in the DSC curves correspond to the glass transition temperature, T_g, and endothermic peaks labeled T_C correspond to the crystallization of the glasses. The values for T_g exhibit only a slight increase from 629 to 635 K for BF_{10} to MF_{10}, respectively. Similarly, the values for parameter proportional to the resistance of the glass against crystallization, $(T_C - T_g)$, show the highest values for MF_{10} glass, Table 1.

Fig. 2 presents the optical absorption spectra of the studied glasses recorded at room temperature in the wavelength region 300–1050 nm. The absorption edge observed at 329 nm for the glass sample MF_{10} exhibited spectrally red shift when MgO is added to the base Na_2SO_4—P_2O_5 glass. From the observed absorption edges, the optical band gaps (E_o) have been evaluated by drawing Tauc plots between $(\alpha\hbar\omega)^{1/2}$ and $\hbar\omega$ as per the equation:

$$\alpha(\omega)\hbar\omega = c(\hbar\omega - E_o)^2 \quad (1)$$

From the extrapolation of the linear portion of the curves in inset of Fig. 2, the values of optical band gap (E_o) are determined and presented in Table 2. The value of E_o is found to be the lowest for BF_{10} glass. Additionally, the spectrum of MF_{10} glass exhibits three distinct kinks in the edge of UV region at 361, 369 and 376 nm and two well resolved bands at 399 and 419 nm. With the addition of CaO or BaO, these bands are shifted to lower wavelength exhibiting spectrally blue shift with a decrease in intensity. The spectra of all the three glasses show a significant band in the NIR region at about 1000 nm. The summary of the data on optical absorption spectra of these glasses is listed in Table 2.

X-band ESR spectra of present glasses recorded at room temperature are shown in Fig. 3. The spectra display an intense spectral line centered at about $g \approx 2.012$. The intensity of this signal is observed to be the maximal in the spectrum for MF_{10} glass. Also, the spectra exhibited a weak signal at about $g \approx 4.470$. The results for ESR spectra are summarized in Table 3.

The Raman spectra of glasses exhibited several symmetrical and asymmetrical vibrational bands due to P—O, PO_2, PO_3 and PO_4 groups, Fig. 4. All glasses have similar Raman spectra and the details of various band positions and their assignments [26,27] are listed in Table 4. The structural units in phosphate network are usually classified according to the Q^n notation, where n (n = 0–3) represents the number of bridging oxygen atoms per PO_4 tetrahedron.

The Raman band at about 1333 cm^{-1} is due to the stretching mode of terminal oxygen, P=O, whereas band at 1271 cm^{-1} is associated with (PO_2) asymmetric stretching mode in Q^2 confirming a

Author's personal copy

Table 1
Physical parameters of Na_2SO_4—MO—P_2O_5:Fe_2O_3 glasses.

Glass	D (g cm^{-3})	N_i (10^{20} Fe ions/cm^3)	R_i (Å)	R_p (Å)	T_g (K)	$T_c - T_g$ (K)
BF_{10}	2.849	2.63	15.62	6.29	629	269
CF_{10}	2.525	2.53	15.80	6.37	631	270
MF_{10}	2.511	2.41	16.07	6.48	635	271

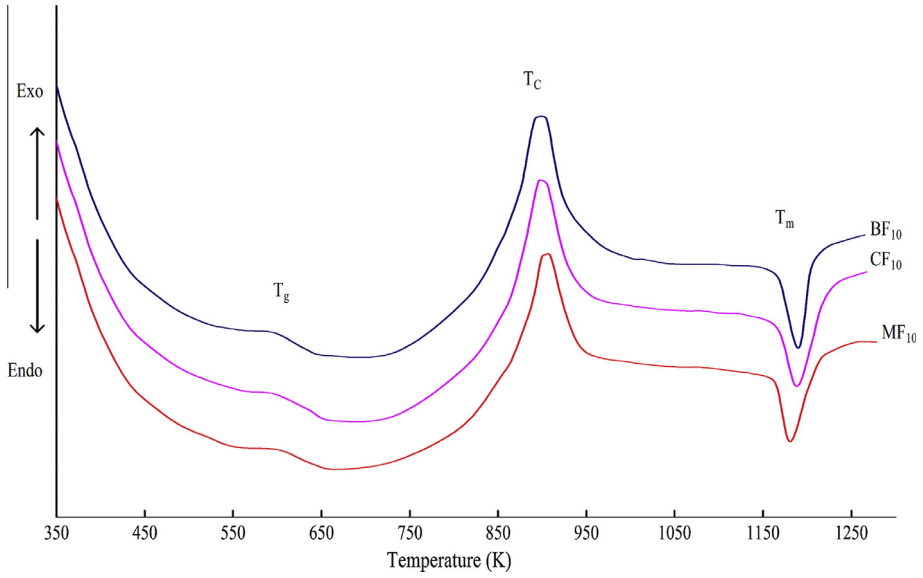

Fig. 1. DSC traces of Na_2SO_4—MO—P_2O_5:Fe_2O_3 glasses.

Table 2
Principal data on optical absorption spectra Na_2SO_4—MO—P_2O_5:Fe_2O_3 glasses.

Glass	Cut-off wavelength (nm)	Band positions (nm) $^6A_{1g}(S) \rightarrow$						Optical band gap (eV)
		$^4E_g(D)$	$^4T_{2g}(D)$	$^4T_{1g}(G)$	$A_{1g}(G)/^4T_{1g}(P)^4$	$^4E_g(G)$	$^5T_{2g} \rightarrow {}^5E_g$	
BF_{10}	340	357	363	371	393	412	1005	3.63
CF_{10}	337	360	366	374	396	415	1001	3.68
MF_{10}	329	361	369	376	399	419	998	3.73

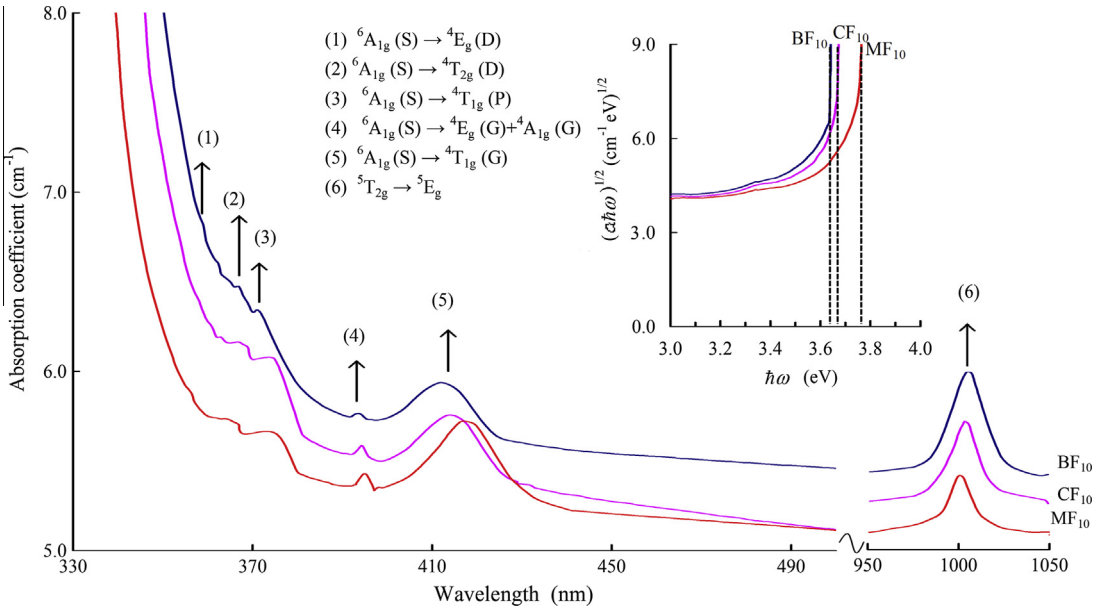

Fig. 2. Optical absorption spectra of Na_2SO_4—MO—P_2O_5 glasses doped with Fe_2O_3. Inset represents Tauc plots of different modifier glasses.

Author's personal copy

Table 3
ESR spectra of Na_2SO_4—MO—P_2O_5:Fe_2O_3 glasses.

Glass	g-Factors	
	Signal-1	Signal-2
BF_{10}	2.016	4.470
CF_{10}	2.013	4.465
MF_{10}	2.008	4.459

significant degree of double-bond character in metaphosphate structure. Intensive band at about 1170 and less intensive band at 1116 cm^{-1} are attributed to the P—O stretch, chain terminator, in Q^2 and Q^1, respectively. These two bands imply a bond order intermediate between those of Q^2 and Q^1 tetrahedra.

Both bands at about 1051 and 1003 cm^{-1} originate from the symmetric modes. The 1051 cm^{-1} band is due to the motion of the non-bridging oxygens (PO_3) in Q^1 tetrahedra whereas the 1003 cm^{-1}, band is assigned to the symmetric stretching mode of non-bridging oxygens in Q^0 phosphate tetrahedra. The Raman band at about 911 cm^{-1} is due to the asymmetric stretching mode of non-bridging oxygens (PO_4) in Q^0 tetrahedra. The 692 and 756 cm^{-1} bands are assigned to the motion of bridging oxygen (P—O—P) in Q^2 and Q^1 tetrahedra, respectively.

At low frequencies, the bands in the range 534–390 and 564 cm^{-1} can be assigned to overlapping cations motion vibrations with the deformation modes in phosphate units. The bands at around 564 and 534 cm^{-1} may be due to the bending mode related to the chain motion and M-phosphate network or M—O bond, respectively. The bands which occur at lower frequencies at 468 and 390 cm^{-1} are difficult to accurately assign owing to perturbation by cation motion vibrations and strong dependence upon chain conformation.

The intensity of all the asymmetrical bands is observed to be the highest in the spectrum of BF_{10} glass, whereas, that of symmetrical bands is found to be the highest in the spectrum of MF_{10} glass.

It should be noted that the O/P ratio for glasses investigated is about 2.76 for MF_{10} glass and 2.84 for BF_{10} glass classifying their network between ultraphosphate and metaphosphate structure. However, Raman spectra exhibit bands that correspond to various polyphosphate units present in the network of these glasses. In the other word, the atomic O/P ratio predicts that only Q^2 tetrahedra will exist in these glass compositions. The excess of Q^1 and Q^0 sites

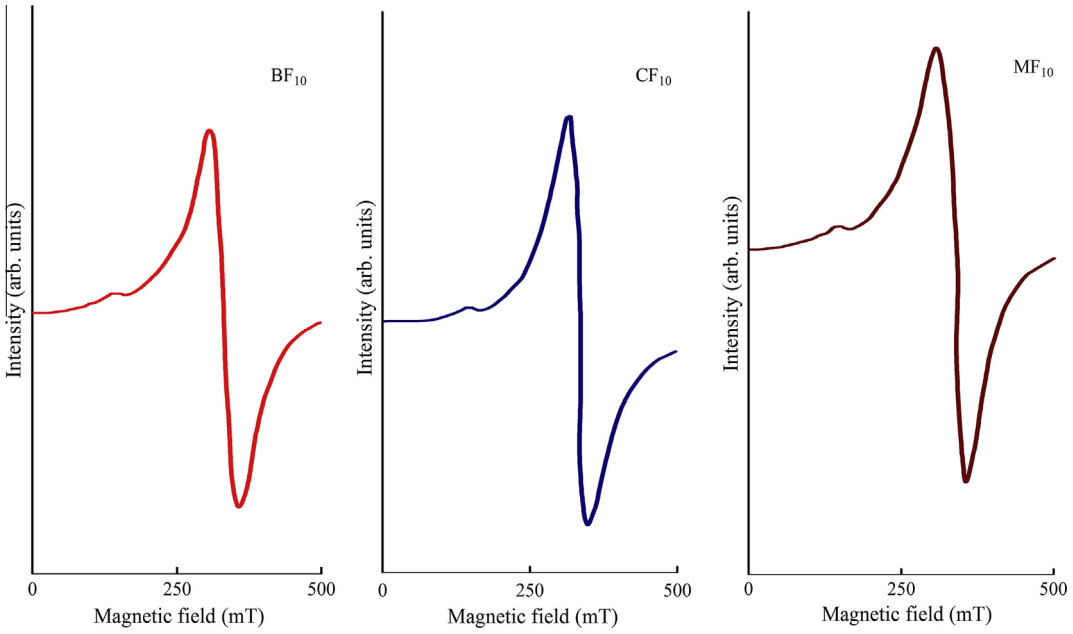

Fig. 3. ESR spectra of Fe_2O_3 doped Na_2SO_4—MO—P_2O_5 glasses recorded at room temperature.

Table 4
Summary of the Raman positions for Na_2SO_4—MO—P_2O_5:Fe_2O_3 glasses (assignment of band positions in cm^{-1}).

Band No.	Assignment	BF_{10}	CF_{10}	MF_{10}
1	Bending mode of phosphate polyhedra with MO modifier	390	393	396
2	PO_4 bending mode in Q^0	468	474	477
3	Bending mode related to the M-phosphate network or M—O bond	534	532	530
4	Bending mode related to the chain motion and chain conformation of phosphate groups	564	560	559
5	$(POP)_{sym}$ stretch in Q^2	692	686	689
6	$(POP)_{sym}$ stretch in Q^1	756	751	749
7	$(PO_4)_{asym}$ stretch in Q^0	911	913	916
8	$(PO_4)_{sym}$ stretch in Q^0 (NBO)	1003	1009	1006
9	$(PO_3)_{sym}$ stretch in Q^1 (NBO)	1051	1049	1046
10	$(PO_2)_{sym}$ stretch in Q^1, chain terminator	1112	1110	1108
11	$(PO_2)_{sym}$ stretch in Q^2, chain terminator	1170	1163	1161
12	$(PO_2)_{asym}$ stretch in Q^2	1271	1271	1275
13	$(P{=}O)_{sym}$ stretch	1333	1330	1328

Author's personal copy

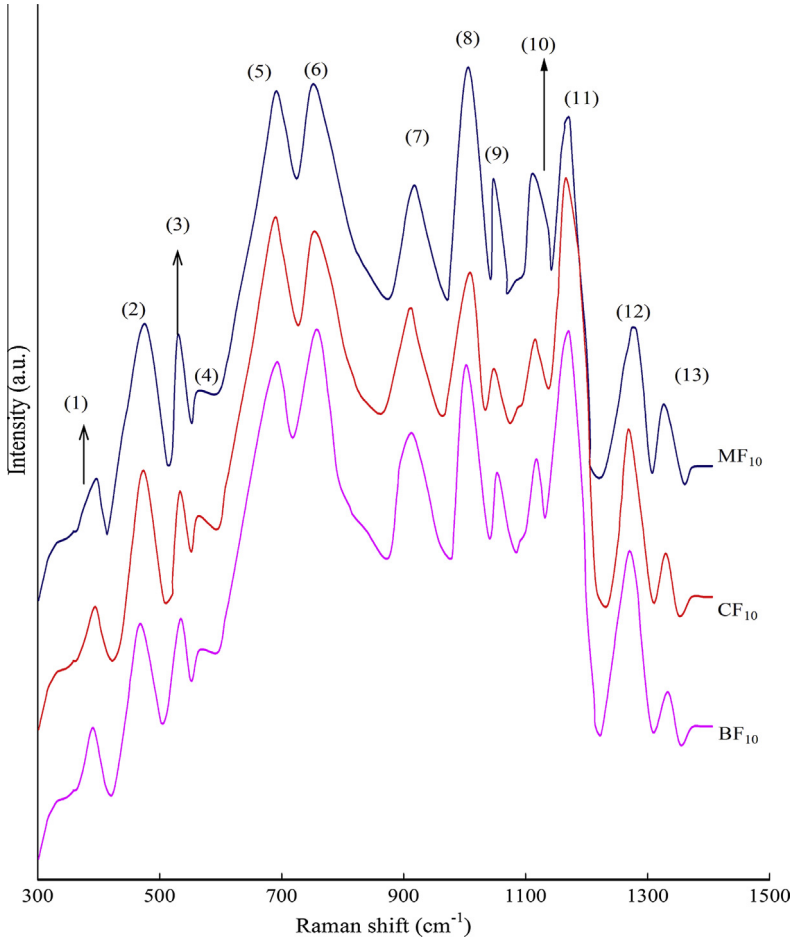

Fig. 4. Raman spectra of Na_2SO_4—MO—P_2O_5:Fe_2O_3 glasses.

Table 5
Data on dielectric loss and relaxations of Na_2SO_4—MO—P_2O_5:Fe_2O_3 glasses.

Glass	$(\tan\delta)_{max.avg.}$	A.E. for dipoles W_d (eV)	Relaxation time, $\tau_{M''}$ (μs)[a]	Relaxation time, $\tau_{Z''}$ (ms)[a]	$\frac{4\pi N\mu^2}{9k_B}$
BF_{10}	149	0.997	11	21	29.5
CF_{10}	41	1.012	26	53	21.3
MF_{10}	45	1.119	14	26	25.6

[a] At 523 K.

observed for these glasses apparently results from the disproportion of Q^2 species in the melt [28].

3.2. Dielectric and electrical properties

The variation of dielectric permittivity, $\varepsilon'(\omega)$, for the CF_{10} glass as a function of frequency at different temperatures is presented in Fig. 5. At higher frequencies, $\varepsilon'(\omega)$ approaches a constant value, $\varepsilon'_\infty(\omega)$, which results from rapid polarization processes occurring in the glasses under applied field [29] and with decreasing frequency, $\varepsilon'(\omega)$ increases and reaches a low-frequency plateau, $\varepsilon'_s(\omega)$, usually associated with the polarization effects of the mobile ions and structural defects with respect to the immobile glass matrix. A strong increase in $\varepsilon'(\omega)$ at lowest frequencies is caused by interfacial phenomenon called the electrode polarization. The observed electrode polarization results from the presence of metallic electrodes, which do not permit transfer of mobile ions into the external circuit. Consequently, ions are accumulated near the electrode causing large polarization of the glass.

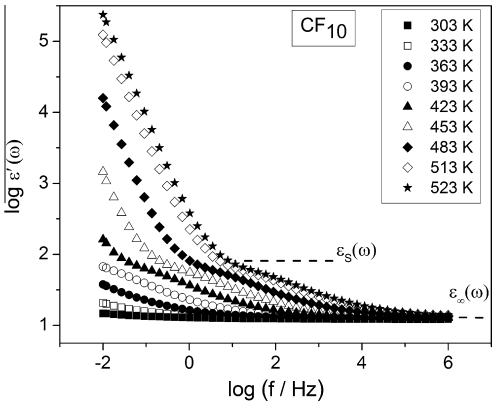

Fig. 5. The variation of dielectric permittivity, $\varepsilon'(\omega)$, for the CF_{10} glass as a function of frequency at different temperatures.

Author's personal copy

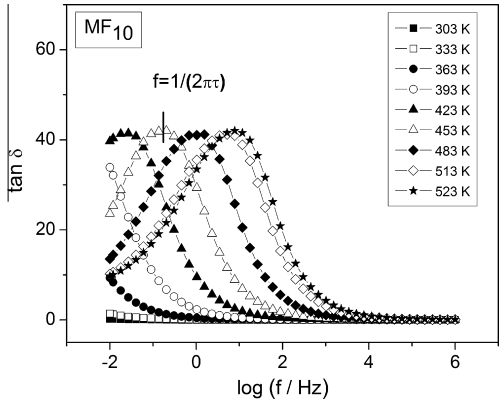

Fig. 6. The variation of dielectric loss, tan δ, with frequency at different temperatures for MF_{10} glass.

The variations of dielectric loss, tan δ, with frequency at different temperatures for MF_{10} glass is presented in Fig. 6. The maximum in the tan δ shifts towards higher frequency with increasing temperature indicating a thermally activated dielectric relaxation [29–32]. Nature of the variation of the dielectric parameters with frequency and temperature is found to be similar for all glasses in this study. In general, the dielectric losses at high frequency are much lower than those occurring at low frequencies at specific temperature. This kind of dependence of tan δ is typically associated with losses by conduction. Using relation $f = f_0 \exp(-W_d/k_BT)$, where f_0 is the constant, k_B is the Boltzmann constant, T is the absolute temperature and f is the relaxation frequency, the effective activation energy for dipoles, W_d, is calculated for all glasses by drawing the plots of log f vs. $1/T$. The activation energy, W_d, is found to be the lowest for the BF_{10} glass, Table 5.

In the ionically conducting glasses, the real part of ac conductivity is well described by the power law in the form:

$$\sigma(\omega) = \sigma_{dc} + A\omega^s \tag{2}$$

where A is the temperature dependent constant and s is the power law exponent $0 < s < 1$ which represents the ion transport characterized by the forward-backward hopping process.

In Fig. 7(a) the ac conductivity, σ_{ac}, as a function of inverse temperature at different frequencies for CF_{10} glass is presented. The inset to Fig. 7(a) exhibits the variation of σ_{ac} conductivity with $1/T$ measured at 1.02 kHz for all glasses studied. The activation energy, W_{ac}, for each glass was determined from the slope of log σ_{ac} vs. $1/T$ curves in the high temperature region over which a linear dependence is observed. The comparison shows the highest value of for the BF_{10} glass measured at 393 K whereas the value of activation energy, W_{ac}, slightly decreases for glasses containing MgO and CaO, as can be seen in Table 6.

The behavior of the s factor is usually related to the ion motion in disordered materials and interpreted by Jonscher [31] as universal dynamic response (UDR). Fig. 7(b) shows the s factor values determined for each glass composition at various temperature. At low temperature s factors exhibits high values while with increasing temperature s decreases and tends to level off in the neighborhood of about 0.60.

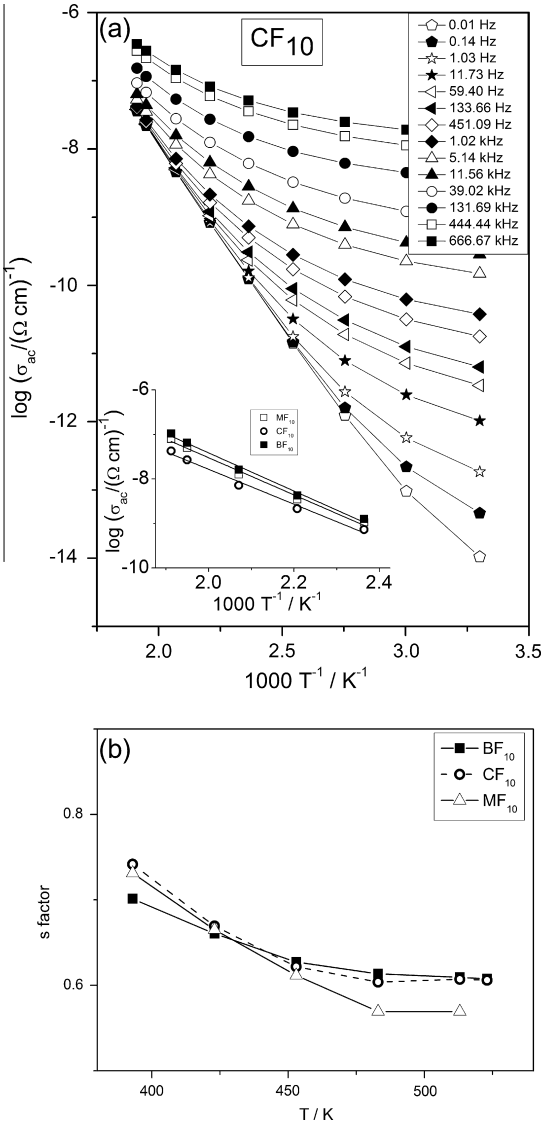

Fig. 7. The variation of ac conductivity with $1/T$ for the glass CF_{10} at different frequencies. Inset represents the comparision plot of the variation of σ_{ac} vs $1/T$ for the three glasses at a frequency of 1.02 kHz (a); temperature variation of exponent s for Na_2SO_4—MO—P_2O_5:Fe_2O_3 glasses (b).

Table 6
Summary of data on ac conductivity for Na_2SO_4—MO—P_2O_5:Fe_2O_3 glasses.

Glass	σ_{ac}[a] $(\Omega\,cm)^{-1}$	W_{ac}[b] (eV)	Exponents[c]
BF_{10}	4.57×10^{-10}	0.85	0.70
CF_{10}	2.80×10^{-10}	0.78	0.74
MF_{10}	3.81×10^{-10}	0.83	0.73

[a] At 1.02 kHz and 393 K.
[b] At 1.02 kHz.
[c] At 393 K.

Table 7
Summary of the data related to dc conductivity of Na_2SO_4—MO—P_2O_5:Fe_2O_3 glasses.

Glass	σ_{dc}[a] $(\Omega\,cm)^{-1}$	log $(\sigma_0/(\Omega\,cm)^{-1}\,K)$	W_{dc} (eV)
BF_{10}	4.86×10^{-11}	5.86	1.06
CF_{10}	1.40×10^{-11}	5.82	1.10
MF_{10}	2.98×10^{-11}	6.03	1.09

[a] At 393 K.

An alternative formalism that may be used for analyzing electrical relaxation behavior in glasses is the electrical modulus [33]. Although there is a debate [34] about the suitability of this formalism, its advantage is that the electrode polarization effects are minimized [35]. In the modulus representation, an electrical modulus M^* is defined as the reciprocal of the complex dielectric constant ε^*:

$$M^*(\omega) = 1/\varepsilon^*(\omega) = \varepsilon'(\omega)/((\varepsilon'(\omega))2 + (\varepsilon''(\omega))^2) + i\varepsilon''(\omega)/((\varepsilon'(\omega))^2 + (\varepsilon''(\omega)^2) = M'(\omega) + iM''(\omega) \tag{3}$$

Author's personal copy

The real and imaginary parts of electrical modulus, $M'(\omega)$ and $M''(\omega)$, as a function of frequency for the MF_{10} glass are presented in Fig. 8(a) and (b), respectively. These figures clearly exhibit the relaxation feature for dielectric properties of the studied glasses. It should be noted that the $M'(\omega)$ increases with increasing frequency and at sufficiently high frequency reaches a plateau which corresponds to the limiting value of $M'(\omega)$. The maximum in the $M''(\omega)$ peak is shifted to higher frequency with increasing temperature. The frequency region below peak maximum $M''(\omega)$ determines the range in which charge carriers are mobile on the long distances. At frequency above peak maximum $M''(\omega)$, the carriers are spatially confined to the potential wells, being mobile on short distances making only localized motion within the wells. From the characteristic frequency, which is equal to the relaxation frequency at which the maximum $M''(\omega)$, occurs, given by $\omega_{max} = 1/\tau_{M''} = \sigma_{dc}/\varepsilon_o\varepsilon'_\infty(\omega)$, the conductivity relaxation time, $\tau_{M''}$, can be extracted as shown in Fig. 8. The relaxation times, $\tau_{M''}$, for all glasses determined at 523 K indicates the lowest value for BF_{10} glass, Table 5.

The conduction relaxation mechanism for all glasses under study is also investigated by the imaginary part of the complex impedance, $Z''(\omega)$. The maximum of the $Z''(\omega)$ spectrum is associated with the contribution of the bulk properties of glasses and usually is at lower frequency with respect to $M''(\omega)$ maxima. The imaginary part of modulus $M''(\omega)$ is compared with $Z''(\omega)$ in Fig. 9. Characteristic relaxation times determined from the maximum of $Z''(\omega)$ are listed in Table 5.

Fig. 10 shows the comparison of the impedance spectra for MF_{10}, CF_{10} and BF_{10} glasses evaluated at 523 K. The spectra for all glasses exhibited depressed semicircles followed by inclined spur at higher temperatures typical for electrode polarization. The equivalent circuit that represents such semicircle is a parallel combination of resistor (R) and constant-phase element (CPE) representing bulk properties, in series with constant-phase element (CPE_{dl}) representing double layer of ions blocked at the electrode surface.

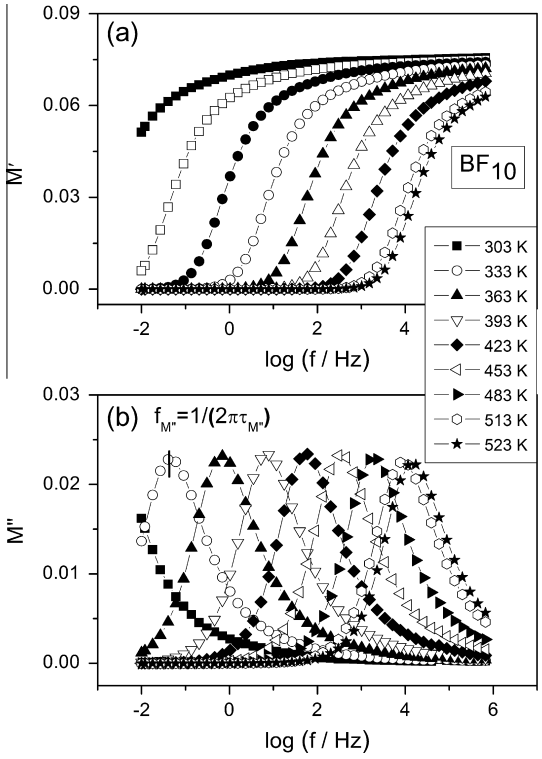

Fig. 8. The frequency dependence of (a) $M'(\omega)$ and (b) $M''(\omega)$ at different temperatures for BF_{10} glass.

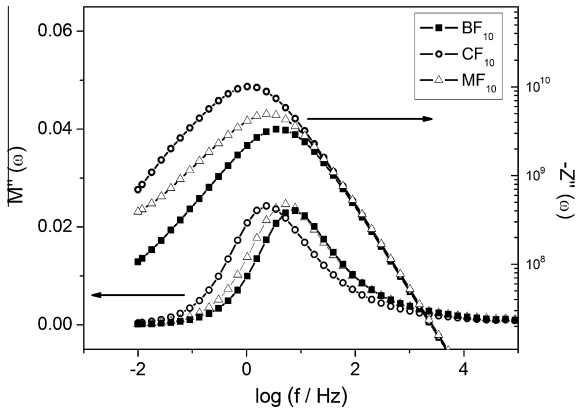

Fig. 9. The frequency dependence of M″(ω) and Z″(ω) at 393 K for Na_2SO_4—MO—P_2O_5:Fe_2O_3 glasses.

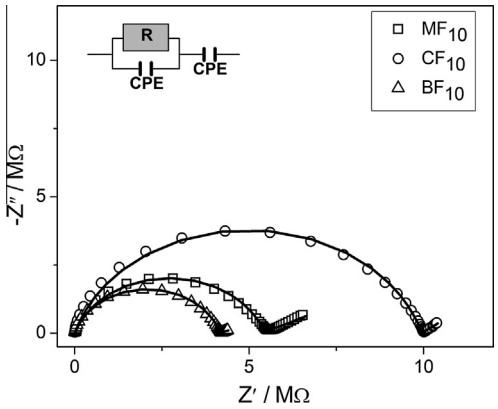

Fig. 10. Impedance spectra for Na_2SO_4—MO—P_2O_5:Fe_2O_3 glasses at 523 K and the corresponding equivalent circuit used for fitting of the data. Circles denote experimental values, solid line corresponds to the best fit.

The values of dc resistance, R, obtained from the modeling and the sample dimensions (d is the sample thickness and A is the electrode area) were used to calculate dc conductivity, $\sigma_{dc} = d/(R \cdot A)$. The activation energy for dc conductivity, W_{dc}, for each glass was determined from the slope of log ($\sigma_{dc} \cdot T$) vs. $1/T$ using equation $\sigma_{dc}T = \sigma_o \exp(-W_{dc}/k_BT)$, where σ_o is the pre-exponent, k_B is the Boltzmann constant and T is the temperature (K). The evaluated dc conductivity variation for all investigated glasses is shown in Fig. 11(a) while the values for the activation energies, W_{dc}, are included in Table 7. Fig. 11(b) shows the compositional dependence of dc conductivity, σ_{dc}, at 393 K and activation energy, W_{dc}. The dc conductivity, σ_{dc}, for glasses containing CaO exhibits the values slightly lower than that for MF_{10} and BF_{10} glasses. Similarly the activation energy, W_{dc}, changes slightly from 1.06 eV for BF_{10} to 1.10 eV for CF_{10}.

4. Discussion

Iron ions may exist in both Fe^{2+} and Fe^{3+} states in the glasses under study. According to our experimental conditions, the reducing agent in the glass melt was provided by H_2 owing to the formation of NH_3 from $(NH_4)H_2PO_4$ salt and its further decomposition into H_2 and N_2 which allow some amount of Fe^{3+} ions in the melted mixtures to reduce to Fe^{2+} ions. Further, phosphate matrix has also a higher reducing effect on the transition metal [36] because of its ability to accept O^{2-} ion.

The Fe^{3+} ions are expected to occupy both tetrahedral and octahedral substitutional positions in these glass networks.

Author's personal copy

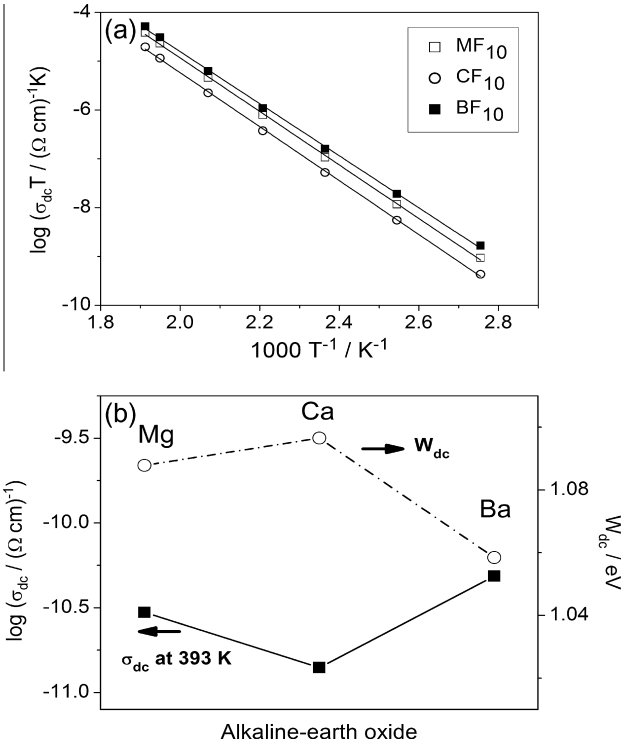

Fig. 11. The variation of dc conductivity, $\sigma_{dc}T$, with $1/T$ for Na_2SO_4—MO—P_2O_5 glasses doped with Fe_2O_3 (a); the compositional dependence of σ_{dc} at 393 K, and activation energy, W_{dc} (b).

Considering that the minimum ratio for the ionic radii of a cation in tetrahedral coordination is 0.19 and in hexagonal coordination is 0.414, it is expected, from the following ratio of cation-oxygen radius of 0.63 (Fe^{2+}) that the Fe^{2+} ion is in hexagonal coordination since the tetrahedral site is more difficult for its occupancy [37]. Therefore, the Fe^{2+} ions are more likely to be found in octahedral or interstitial positions and act as modifiers similar to Na^+ [37]. It should be noted that as interstitial are denoted those Fe^{2+} and Fe^{3+} ions which are attracted by negatively charged glass forming structural units for local charge compensation.

The major constituent of Na_2SO_4—MO—P_2O_5:Fe_2O_3 glass system is the P_2O_5 which participates in the glass network forming the clustered region with various phosphate structures. The PO_4 tetrahedra are linked together with covalent bonding in chains or rings. The chains or rings of phosphate units are subjected to modifications to various extents depending upon the nature of the modifier ions and MO/P_2O_5 ratio. Hence truncated chains, as found in the Raman spectra, Fig. 5, in which a fraction of the phosphate tetrahedra possess three unshared oxygen corners produce the structure. These tetrahedra can be written as $[POO_{2/2}O]^-$ with two bridging oxygens and $[POO_{1/2}O_2]^{2-}$ with one bridging oxygen. The two bridging and one bridging oxygen phosphate groups in the presence of the modifier oxide, respectively, can be written as

$$2\ [POO_{3/2}]^0 + MO \rightarrow 2\ [POO_{2/2}O]^- + M^{2+}$$

$$2\ [POO_{2/2}O]^- + MO \rightarrow 2\ [POO_{1/2}O_2]^{2-} + M^{2+}$$

As previously reported [38], with the combination of Na_2SO_4 and P_2O_5 a formation of the glass with moderate level of sulfur species is possible if the phosphate network contains $[POO_{2/2}O]^-$ and $[POO_{1/2}O_2]^{2-}$ structural units. Further, the results from Raman spectra make it clear that the various phosphate units (Q^2, Q^1 and Q^0) exist in these glasses. While the glass modifiers ions Na^+ and M^{2+} (Ba^{2+}, Ca^{2+}, Mg^{2+}) are shared between various glass former units the modification of the phosphate network is also characterized by disproportion reaction that occurs during reorganization of glass melt [28].

The concentration of various glass former species in the glass network, however, depends upon the nature of the modifier (M^{2+}) ions. In other words, the atomic arrangement at short and intermediate range in the glass network can be considered as a decisive factor for the electrical characteristics of the glass. Following the order of the ionic size or radius of the three modifier ions ($r^{2+}_{Mg} = 0.66$ Å $< r^{2+}_{Ca} = 0.99$ Å $< r^{2+}_{Ba} = 1.34$ Å), one can understand that the replacement of MgO successively by CaO or BaO, causes an increase in the disorder degree of the glass network. Further, since the ionic radius of Fe^{2+} ion is $r^{2+}_{Fe} = 0.74$ Å, the closer value to r^{2+}_{Mg} suggests that the probability for the substitutional positioning of Fe^{2+} ions is higher in MgO containing glass, whereas occupancy of interstitial positions is higher for Fe^{2+} ions in BaO containing glass. Thus, the change of the modifier oxide causes structural modifications at the dopant iron ions site in Na_2SO_4—P_2O_5:Fe_2O_3 glass network. However, it is worth noting that there is only 1 mol% of Fe_2O_3 in the glasses studied, so the concentration of Fe^{2+} ions which can participate either in interstitial or substitutional position is low.

If we consider the varying modifier ions to be incorporated between the long-chain molecules in the vicinity of dopant ion in the phosphate network, then the local symmetry and/or covalency of the glass at the iron ions might be slightly different for different modifiers in the glass network. Additionally, the variations in the concentration of various structural units of phosphate and linkages between them are also expected to modify the crystal field around iron ions in the glass network. Overall, there is a higher degree of structural depolymerization in the glasses with BaO as modifier when compared with other two glass systems. The lowest values of glass transition temperature T_g and $T_C - T_g$ observed in DSC studies for BaO containing glass indicates lower cross-link density of various structural groups and weakening of glass network.

The observed bands in the optical absorption spectra are conventional bands originated from the ground state $^6A_{1g}$ to some quartet states and these are both spin and parity forbidden. Using Tanabe-Sugano energy level diagram for d^5 configuration, the bands observed at 361, 369, 376, 399 and 419 nm in the optical absorption spectra of MF_{10} glasses are assigned to $^6A_{1g}$ (S) → ^4E_g (D), $^4T_{2g}$(D), $^4T_{1g}$(P), $^4A_{1g}$(G)+ ^4E_g(G) and $^4T_{1g}$ (G) octahedral transitions of Fe^{3+} ions, respectively [39–42]. Since all the excited states are spin quartet states, no spin allowed transitions would occur for Fe^{3+} ions. Hence, Fe^{3+} ions are characterized by weak bands, which arise due to the spin forbidden transitions. However, the transition $^6A_{1g}(S) \rightarrow {}^4T_{1g}(G)$ involves a change of configuration from $(t_{2g})^3(e_g)^2$ to $(t_{2g})^4(e_g)^1$ and is therefore expected to be relatively broader as observed. The broad peak observed at around 1000 nm is due to $^5T_{2g} \rightarrow {}^5E_g$ octahedral transition of Fe^{2+}. The peak positions of all the Fe^{3+} bands exhibited spectrally blue shift with a considerable decay of intensity as the modifier MgO is replaced by CaO and BaO. However, the band due to Fe^{2+} ions exhibited a reversal trend.

The validity of the Eq. (1) between $(\alpha\hbar\omega^{1/2}$ and $\hbar\omega$ points out that the optical band gap is caused by amorphous optical absorption edge. This indicates the fact that the disordered amorphous glass materials have prevailingly the direct transitions between the valence band and the conduction band and the absence of the indirect inter-band transitions like in the case of the crystals (i.e. the transitions in the different points of the Brillouin zone). Some deviations observed from this dependence are understood due to trapping of some disordered states within the energy gap. The lowest value of optical band gap (E_o) obtained for BF_{10} glass, Table 2, suggests a higher amount of the depolymerization or more bonding defects and non-bridging oxygens (NBO) in the BF_{10} glass network.

Author's personal copy

The optical activation energy associated with $^6A_{1g}(S) \rightarrow {}^4T_{1g}(G)$ octahedral band of Fe^{3+} ions is increased from 2.96 eV (glass BF_{10}) to 3.01 eV (glass MF_{10}), whereas the energy of Fe^{2+} ion transition band is decreased from 1.25 eV to 1.23 eV for the substitution of other modifier ion. This is clearly a characteristic feature for inter-valence transfer or a polaronic type of absorption. It means that the associated electrons are trapped at shallow sites within the main band gap (in BF_{10} glass) and as a consequence possess smaller effective wave-function radii. This kind of situation is only possible if the local potential fluctuation is small with respect to transfer integral, j. A small overlap between electronic wave functions (corresponding to adjacent sites) due to strong local disorder is contributive to polaron formation. So, within a framework of polaronic model, the electron delivered by the impurity atom at the Fe^{3+} site converts this one into a lower valence state Fe^{2+}. Afterwards the trapped electron at this Fe^{2+} site is transferred to the neighboring new Fe^{3+} site by absorbing a photon quantum. Thus the optical absorption in the glass samples is dominated by polaronic transfer between the Fe^{2+} and Fe^{3+} species in BF_{10} glasses [43,44].

In the ESR spectra, the spectral line centered at $g \approx 4.470$ is identified as being due to the isolated Fe^{3+} ions in sites of distorted octahedral symmetry (orthorhombic) subjected to strong crystal field, while the line at $g \approx 2.016$ is attributed to the isolated Fe^{3+} ions in a less distorted structural unit or due to Fe^{3+}—O—Fe^{3+} exchange coupled pairs.

It is interesting to remark that in the case of studied glasses the line at $g \approx 4.4$ due to isolated Fe^{3+} ions appeared but exhibits a low intensity. It can be concluded that at small content of Fe_2O_3 (1 mol%), the Fe^{3+} ions are not disposed in the glass network by playing the role of the network former or modifier, but they are disposed in the sites easier to occupy, offered by the matrix. It seems that these sites are relatively large and allow the association of Fe^{3+} ions even at such small content of Fe_2O_3, suggesting that they are not isolated and situated in sites of distorted octahedral symmetry. This is consistent with previously reported EPR and magnetic studies for various phosphate glasses doped with iron ions [45,46].

The intensity ($\Im$) of the EPR signal is evaluated using $\Im \approx I(\Delta B)^2$, where I is the peak-to-peak height and ΔB is the square of width of the signal [47] for $g_{eff} \approx 2.016$ resonance appears to be the lowest for BF_{10} glass. The spectral line at $g \approx 2.016$ reveals different possibility of interaction of the iron ions in the investigated glasses. The ΔB dependence suggests the competition between the broadening mechanisms such as the dipole–dipole interaction, the increased disordering of the glass structure, interaction between ions in multivalent states and exchange interactions within the pairs of iron ions. The former shifts the resonance field of any given ion by an amount representing the average magnetic fields (both static and dynamic) due to all the other magnetic ions in the solid. This is termed inhomogeneous broadening and often results in a Gaussian line shape. Exchange interactions result from mutual spin flipping, which under some circumstances can tend to average out the local dipolar fields, leading to line narrowing [48]. The final line width depends on the relative strengths of both the mechanisms. The slightly higher value of g_{eff} obtained for the BF_{10} glasses indicates some dipolar interaction that causes a localized magnetic field at the site of Fe^{3+} ion.

The dielectric and electrical data of such a complicated Na_2SO_4—MO—P_2O_5:Fe_2O glass system is discussed in several directions. At a given frequency and temperature dielectric parameters viz., $\varepsilon'(\omega)$, $\tan\delta$ and σ_{ac} are found to be the highest for BF_{10} glass. In general electronic, ionic, dipolar and space charge polarizations contribute to the dielectric constant. Among these, it is the space charge polarization (which depends upon the concentration of defects in the glass network) that influences strongly the dielectric permittivity at lower frequencies. As mentioned earlier, there is a possibility that even at low content of Fe_2O_3 (1 mol%) the Fe^{2+} ions similarly to the Na^+, Ba^{2+}, Ca^{2+} and Mg^{2+} ions may act as modifiers creating the dangling bonds and nonbridging oxygens by disrupting phosphate chains. Thus, the defects produced create an easy pathway for the migration of charges that would build up space charge polarization and facilitate to an increase in the dielectric parameters [49–51]. The decreasing trend of dielectric parameters with the successive replacement of Ba^{2+} ions by Ca^{2+} or Mg^{2+} ions suggests increasing degree of electrical rigidity in the glass network.

The Debye model is related to an ideal frequency response of localized relaxation. In reality the non-localized process is dominated at low frequencies. In the absence of interfacial effects, the non-localized conductivity is known as the dc conductivity. Thus, the high dielectric loss, $\tan\delta$, is usually accompanied by rising $\varepsilon'(\omega)$ at low frequencies. Such behavior is found for the present glasses and showed in Fig. 5. However, it should be noted that the localized relaxation process has much smaller values of $\varepsilon'(\omega)$ and τ than the non-localized one.

The effect of Ba^{2+}, Ca^{2+} and Mg^{2+} addition on the relaxation mechanisms of Na_2SO_4—P_2O_5:Fe_2O glasses was also investigated by both $Z''(\omega)$ and $M''(\omega)$ as a function of frequency, Fig. 10. Comparison with the impedance and electrical modulus data allow the determination of the bulk response in terms of localized, i.e. defect relaxation or non-localized conduction, i.e. ionic conductivity [52]. There are two apparent relaxation regions in $M''(\omega)$ peak, the low-frequency region, being associated with the hopping conduction and high-frequency region being associated with the relaxation polarization process. For the present glasses the $M''(\omega)$ and $Z''(\omega)$ peaks do not completely overlap but are very close suggesting the components from both long-range and localized relaxation and distribution of relaxation times [53].

At the characteristic frequency of the maximum of $M''(\omega)$ and $Z''(\omega)$ the relaxation times $\tau_{M''}$ and $\tau_{Z''}$ are extracted and listed in Table 5. Although there is a small difference between glasses, it is clear that at any chosen temperature, the relaxation times, $\tau_{M''}$ and $\tau_{Z''}$ for BF_{10}, exhibit the lowest values. The relaxation times, $\tau_{M''}$, as well as $\tau_{Z''}$, are thermally activated with the following respective activation energy $E_{M''}$. From Table 5 it is clear that the relaxation times, $\tau_{M''}$, for the BF_{10} and MF_{10} glasses are smaller due to a smaller $E_{M''}$ and E_{dc} and consequently, a higher conductivity, σ_{dc}. For the CF_{10} glass the relaxation time, $\tau_{M''}$, become higher because of the enhanced mixed "alkali–alkaline earth effect" [12] which will be discussed in more details later. In addition a close maximum position of $M''(\omega)$ and $Z''(\omega)$ peaks, represented for all three glasses in Fig. 10 illustrates that the dynamic process occurring at different frequencies exhibits the same thermal activation energy. Therefore, both peaks, $M''(\omega)$ and $Z''(\omega)$, describe the same relaxation process.

According to Figs. 7 and 10 the position of the peak in the $\tan\delta$ curve is shifted to a lower frequency region related to the $Z''(\omega)$ and $M''(\omega)$ peaks. These three peaks describe the relaxation process with following order of relaxation time:

$$\tau_{\tan\delta} > \tau_{Z''} \geq \tau_{M''}$$

If it is assumed that the electrical field in these glasses is a Lorenz field, the connection between the number, N, of the dipoles per unit volume, the dipole moment, μ, and the low and high frequency dielectric constants, $\varepsilon'_s(\omega)$ and $\varepsilon'_\infty(\omega)$, can be presented according to Classius–Mosetti Debye relation with modification of Bottcher and Bordewijk [29]:

$$\frac{\varepsilon'_s - 1}{\varepsilon'_s + 2} - \frac{\varepsilon'_\infty - 1}{\varepsilon'_\infty + 2} = \frac{4\pi N\mu^2}{27k_BT} \quad (4)$$

Due to the fact that in the present glasses ions and dipoles can be approximately regarded as mere points and the concentration of dipoles is not abnormally high, one need not doubt the applicability of the Eq. (4). After rearranging the terms, Eq. (4) is modified to:

Author's personal copy

$$\frac{\varepsilon'_s - \varepsilon'_\infty}{(\varepsilon'_s + 2)(\varepsilon'_\infty + 2)} T = \frac{4\pi N\mu^2}{9k_B} \quad (5)$$

The quantity, $N\mu^2$, in the right hand side of Eq. (5) represents the strength of dipoles. Substituting the values of, $\varepsilon'_s(\omega)$ and $\varepsilon'_\infty(\omega)$, the quantity, $4\pi N\mu^2/9k_B$ is evaluated at 523 K for all the three glasses and presented in Table 5. The value of $4\pi N\mu^2/9k_B$ is found to be the highest for BF_{10} glass indicating that the spreading of relaxation times is the highest in this glass when compared with the other two glasses. The spreading of relaxation times is possibly due to the coupling of individual relaxation processes, one site needing to relax before the other can do so. Even if each relaxation site has the same value of τ the coupling between them ensures that the time domain is effectively stretched leading to the spreading of relaxation times as observed [29,54,55]. The possible contributors to the dipolar effects in addition to the octahedral complexes of Fe^{2+} ions are the complexes of divalent alkaline earth ions [56]. The lowest value of activation energy for dipoles and also the relaxation time observed for BF_{10} sample, Table 5, suggests the highest degree of freedom for dipoles to orient in the field direction in this glass network.

Typical ac conductivity spectra at different temperatures are shown in Fig. 8 for CF_{10} glass. The transition point between two regions, dc conductivity and dispersion, is shifted toward higher frequency with increasing temperature. The variation of s values with temperature are exhibited for all glasses under study in Fig. 7(b) and listed in Table 6. The values are higher at low temperatures whereas rapidly decrease with increasing temperature reaching a minimum at about 0.6. The lowest value for s factor found for BF_{10} glass is consistent with more evidenced modified phosphate network containing various phosphate units. This leads to the conclusion that more instable ion sites are formed, which due to opening of many channels, results in an enhanced ion transport over long distance for BF_{10} glass. Moreover, according to Dyre and Schroder [57] the temperature dependence of the s factor was explained on the basis of the many body interaction model. At low temperature the interaction between the neighboring charge carriers is almost negligible. As temperature increases, the interaction increases, leading to a decrease in s. If s increases with temperature the correlated barrier hopping (CBH) mechanism is dominant assuming that the lower values of s occur for multiple hops while the higher values occur for single hops. Clearly the transition between different s regimes is associated with the transition from the low activation barriers to the high activation barrier in conductivity.

The dc conductivity, σ_{dc}, is changed only slightly, less than one order of magnitude, for this series of glasses, Fig. 11(b). However, the highest values of σ_{dc} at any temperature found for BF_{10} glass is probably related to the higher mobility of Na^+ ions in a disordered phosphate network. As earlier pointed out, Ba^{2+} ions do act as modifiers and enhance the concentration of dangling bonds. This in turn causes a decrease in the electrostatic binding energy and the strain energy for the easy passage of Na^+ ions which consequently leads to a substantial decrement in the jump distance. Similar effect is expected for glasses containing Ca^{2+} and Mg^{2+} ions, but the magnitude of induced disorder and fragmentation of the phosphate matrix is much higher in BF_{10} glass. This behavior is in good accordance with the lowest value of activation energy for conduction observed in case of BF_{10} glass when compared with that of the other two glass systems.

On the other hand, the behavior for σ_{dc} is a result of the interactions between Na^+ ions and alkaline-earth (Ca^{2+}, Mg^{2+}, Ba^{2+}) ions due to the "mixed alkali–alkaline-earth" effect. In silicate and phosphate glasses the replacement of alkali by alkaline-earth oxides results in a decrease in conductivity of several orders of magnitude. This effect changes in the order MgO < CaO < BaO, meaning that for a given molar composition, glass containing MgO exhibits the smallest decrease in conductivity [12]. However, since the replacement of one alkaline-earth by another while maintaining the identity of the alkali ion has a much smaller effect on the conductivity [12], an exact glass composition should be specifically considered. The observed lowest value of σ_{dc} in glass MF_{10} is probably caused by the more effective "mixed alkali–alkaline-earth" interactions and also due to the significant modifications of phosphate network in this glass. Nevertheless, it is worth noting that these glasses show very weak variation of conductivity with the changes of the type of the alkaline-earth oxide indicating only slight influence on the transport of Na^+ ions. Although these glasses contain Fe^{2+} and Fe^{3+} ions in a small amount (app. 1 mol% of Fe_2O_3) it is not expected that the polaronic conduction dominates the electrical transport, but some small contribution due to the hopping between Fe^{2+} and Fe^{3+} ions cannot be excluded.

The results from the present study show the different behavior of σ_{ac} and σ_{dc}, Tables 6 and 7, which can be explained by percolation theory [58]. The dc conductivity is a result of a long-range motion of the ions which can take place only when a percolation conductive cluster exists, whereas, the σ_{ac} is related to the ionic motion on shorter length scales and it is not connected with the existence of percolation conductive cluster. As a result, σ_{ac} only slightly depends on the composition and does not show significant change within glasses in this series. Going further in analysis, the activation energies which describe the temperature dependence of σ_{ac} and σ_{dc} is discussed. As a matter of fact, in all cases the activation energy of the ac conductivity is lower than that of the dc conductivity which again reflects that the σ_{ac} probes dynamics on shorter time and length scales. Overall, the ac conductivity for the present glass represents the short range movement of Na^+ ions (and small polarons) and therefore they have to overcome only local activation energy barriers. For the long-range motion related to the dc conductivity the Na^+ ions (and small polarons) have to overcome larger barriers.

5. Conclusions

Sodium sulfo-phosphate glasses mixed with three different modifier oxides (viz., MgO, CaO and BaO) and doped with 1.0 mol% of Fe_2O_3 were prepared. A variety of spectroscopic electrical and dielectric studies have been carried out. The spectroscopic properties have indicated that the iron ions exist in Fe^{3+} and Fe^{2+} states. These results further indicated that Fe^{3+} ions participate in the glass network with tetrahedral occupancy, whereas Fe^{2+} ions mainly act as modifiers. The reduction of iron ions from Fe^{3+} to Fe^{2+} state is found to be more in BaO mixed glasses. The analysis of the results dielectric loss, electric moduli and impedance diagram indicated that there is long-range and localized relaxation and distribution of relaxation times. The possible contributors to the dipolar effects were identified as octahedral complexes of Fe^{2+} ions and the complexes of divalent alkaline earth ions. The distribution of relaxation is observed to be more in case of BaO mixed glasses and it is attributed to the higher degree of disorder in the glass containing as BaO as modifier.

The dc conductivity in these glasses is understood due to the result of a long-range motion of the Na^+ ions (and small polarons) that have to overcome larger barriers ions, whereas, the σ_{ac} is found to be related to the ionic motion on shorter length scales and in this case Na^+ ions (and small polarons) have to overcome only local activation energy barriers. This conclusion is further confirmed by the obtained values of activation energy. The activation energy of the ac conductivity is found to be lower than that of the dc conductivity which reflects that the σ_{ac} probes dynamics on shorter time and length scales. The highest ac/dc conductivity and lowest activation energy for conductivity observed for glasses

Author's personal copy

mixed with BaO modifier. This is attributed to the significant increase of ionic contribution due to an increase in the concentration of dangling bonds that have lead to the substantial decrement in jump distance for sodium ions.

Acknowledgements

One of the authors, N. Veeraiah wishes to thank DST, Govt. of India for supporting this work through FIST programme. A. Mogus-Milancovic wishes to thank the Croatian Ministry for Science, Education for supporting this work through the Grant No: 098-0982929-2916.

References

[1] A. Moguš-Milanković, L. Pavić, K. Srilatha, Ch. Srinivasa Rao, T. Srikumar, Y. Gandhi, N. Veeraiah, J. Appl. Phys. 111 (2012) 013714.
[2] S.M. Salem, E.K.A. Khalek, E.A. Mohamed, M. Farouk, J. Alloys Comp. 513 (2012) 35–43.
[3] R.M.M. Morsi, M.A.F. Basha, Mater. Chem. Phys. 129 (2011) 1233–1239.
[4] M. Shapaan, S.A. El-Badry, A.G. Mostafa, M.Y. Hassaan, M.H. Hazzaa, J. Phys. Chem. Solids 73 (2012) 407–417.
[5] T. Srikumar, I.V. Kityk, Ch. Srinivasa Rao, Y. Gandhi, M. Piasecki, P. Bragiel, V. Ravi Kumar, N. Veeraiah, Ceram. Int. 37 (2011) 2763–2779.
[6] T. Satyanarayana, I.V. Kityk, M. Piasecki, P. Bragiel, M.G. Brik, Y. Gandhi, N. Veeraiah, J. Phys. – Cond. Matter 21 (2009) 245104.
[7] F. Scholz, J. Solid State Electrochem. 15 (2011) 5–14.
[8] C.W. Kim, D.E. Day, J. Non-Cryst. Solids 331 (2003) 20–31.
[9] M. Ganguli, K.J. Rao, J. Non-Cryst. Solids 243 (1999) 251–267.
[10] P.A. Bingham, R.J. Hand, Mater. Res. Bull. 43 (2008) 1679–1693.
[11] W. Vogel, Glass Chemistry, Springer Verlag, Berlin, 1994.
[12] J.E. Shelby, J. Non-Cryst. Solids 263 (2000) 271–276.
[13] P. Bergo, W.M. Pontuschka, J.M. Prison, C.C. Motta, J. Int. Meas. Confederation 43 (2010) 210–215.
[14] L. Zhang, R.K. Brow, J. Am. Ceram. Soc. 94 (2011) 3123–3130.
[15] F.E. Salman, A. Mekki, J. Non-Cryst. Solids 357 (2011) 2658–2662.
[16] P. Pascuta, R. Lungu, I. Ardelean, J. Mater. Sci.: Mater. Electron. 21 (2010) 548–553.
[17] S. Rada, R. Chelcea, E. Culea, J. Mater. Sci. 45 (2010) 6025–6029.
[18] A. Al-Shahrani, A. Al-Hajry, M.M. El-Desoky, Physica B 364 (2005) 248.
[19] B.O. Mysen, J. Non-Cryst. Solids 95&96 (1987) 247–254.
[20] A. Šantić, Ž. Skoko, A. Gajović, S.T. Reis, D.E. Day, A. Moguš-Milanković, J. Non-Cryst. Solids 357 (2011) 3578–3584.
[21] K. Srilatha, K. Sambasiva Rao, Y. Gandhi, V. Ravikumar, N. Veeraiah, J. Alloys Comp. 507 (2010) 391–398.
[22] A. Moguš-Milanković, A. Šantić, S.T. Reis, K. Furić, D.E. Day, J. Non-Cryst. Solids 342 (2004) 97–109.
[23] P. Raghava Rao, N. Venkatramaiah, Y. Gandhi, V. Ravi Kumar, I.V. Kityk, N. Veeraiah, Spectrochim. Acta A 86 (2012) 472–480.
[24] P. Raghava Rao, G. Murali Krishna, M.G. Brik, Y. Gandhi, N. Veeraiah, J. Lumin. 131 (2010) 212–217.
[25] P. Raghava Rao, L. Pavić, A. Moguš-Milanković, V. Ravi Kumar, I.V. Kityk, N. Veeraiah, J. Non-Cryst. Solids 358 (2012) 3255–3267.
[26] R.K. Brow, D.R. Tallant, S.T. Myers, C.C. Phifer, J. Non-Cryst. Solids 191 (1995) 45–55.
[27] C. Nelson, D.R. Tallant, J. Phys. Chem. Glasses 26 (1985) 119–122.
[28] X. Fang, C.S. Ray, A. Moguš-Milanković, D.E. Day, J. Non-Cryst. Solids 283 (2001) 162–172.
[29] C.J.F. Böttcher, P. Bordewijk, Theory of Electrical Polarization, Elsevier, Amsterdam, 1978, pp. 399–406.
[30] N. Krishna Mohan, M. Rami Reddy, N. Veeraiah, J. Alloys Comp. 458 (2008) 66–76.
[31] A.K. Jonscher, Dielectric Relaxation in Solids, Chelsea Dielectric, London, 1996.
[32] V. Ravikumar, N. Veeraiah, S. Buddudu, J. de Phys. III (7) (1997) 951–962.
[33] P.B. Macedo, C.T. Moynihan, R. Bose, J. Phys. Chem. Glasses 13 (1972) 171–179.
[34] D.L. Sidebottom, B. Roling, K. Funke, Phys. Rev. B63 (2000). 024301-1.
[35] A. Šantić, C.W. Kim, D.E. Day, A. Moguš-Milanković, J. Non-Cryst. Solids 356 (2010) 2699–2703.
[36] K. Moringa, H. Yoshida, H. Takebe, J. Am. Ceram. Soc. 77 (1994) 3113–3118.
[37] S.M.D. Nery, W.M. Pontuschka, S. Isotani, C.G. Rouse, Phys. Rev. B49 (1994) 3760–3765.
[38] M. Ganguli, M.H. Bhat, K.J. Rao, Solid State Ionics 122 (1999) 23–33.
[39] W. Hui, K. Xiao-Yu, D. Dong, T. Xiao-Ming, Y. Xiong, Chem. Phys. 330 (2006) 212–215.
[40] I. Fontana, A. Lauria, G. Spinolo, Phys. State Solidi (b) 244 (2007) 4669–4677.
[41] S. Gunasekaran, G. Anbalagan, Spectrochim. Acta A 69 (2008) 383–390.
[42] N.O. Gopal, K.V. Narasimhulu, J.L. Rao, J. Phys. Chem. Solids 65 (2004) 1887–1893.
[43] R.S. Muralidhara, C.R. Kesavulu, J.L. Rao, R.V. Anavekar, R.P.S. Chakradhar, J. Phys. Chem. Solids 71 (2010) 1651–1655.
[44] B.V. Raghavaiah, N. Veeraiah, J. Magn. Magn. Mater. 284 (2004) 363–368.
[45] P. Pascuta, G. Borodi, A. Popa, V. Dan, E. Culea, Mater. Chem. Phys. 123 (2010) 767–771.
[46] R.K. Singh, A. Srinivasan, J. Magn. Magn. Mater. 321 (2009) 2749–2752.
[47] J.W. Fergus, J. Power Sources 162 (2006) 30–40.
[48] J.A. Abragam, B. Bleaney, Electron Paramagnetic Resonance of Transition Ions, Oxford University Press, Belfast, 1970.
[49] A.V. Ravi Kumar, Ch. Srinivasa Rao, T. Srikumar, Y. Gandhi, V. Ravi Kumar, N. Veeraiah, J. Alloys Comp. 515 (2012) 134–142.
[50] A. Moguš-Milanković, V. Ličina, S.T. Reis, D.E. Day, J. Non-Cryst. Solids 353 (2007) 2659–2666.
[51] Ch. Srinivasa Rao, T. Srikumar, Y. Gandhi, V. Ravikumar, N. Veeraiah, Philos. Mag. 91 (2011) 958–980.
[52] R. Gerhardt, J. Phys. Chem. Solids 55 (1994) 1491–1506.
[53] I.M. Hodge, M.D. Ingram, A.R. West, J. Electroanal. Chem. 74 (1976) 125–143.
[54] V. Ličina, A. Moguš-Milanković, S.T. Reis, D.E. Day, J. Non-Cryst. Solids 353 (2007) 4395–4399.
[55] S.R. Elliott, Physics of Amorphous Materials, Longman Sci. & Tech, Essex, 1990.
[56] G. Little Flower, M. Srinivasa Reddya, M. Venkata Ramana Reddy, N. Veeraiah, Z. Naturforsch 62a (2007) 315–323.
[57] J.C. Dyre, T.B. Schroder, Rev. Mod. Phys. 72 (2000) 873–892.
[58] A. Bunde, S. Havlin (Eds.), Fractals and Disordered Systems, Springer, Berlin, 1996.